N. P. Costa
e-mail: ncosta@fe.up.pt

R. Maia
e-mail: rmaia@fe.up.pt

M. F. Proença
e-mail: fproenca@fe.up.pt

Departamento de Engenharia Civil,
Faculdade de Engenharia da Universidade do Porto,
Rua Dr. Roberto Frias,
4200-465 Porto,
Portugal

F. T. Pinho[1]
Centro de Estudos de Fenómenos de Transporte,
Faculdade de Engenharia da Universidade do Porto,
Rua Dr. Roberto Frias,
4200- 465 Porto,
Portugal
and
Universidade do Minho, Largo do Paço, 4704-553 Braga, Portugal
e-mail: fpinho@fe.up.pt

Edge Effects on the Flow Characteristics in a 90 deg Tee Junction

Measurements of pressure drop were carried out for the flow of a Newtonian fluid in 90 deg *tee junctions with sharp and round corners. Rounding the corners reduced the energy losses by between 10 and 20%, depending on the flow rate ratio, due to the reduction in the branching flow loss coefficient, whereas the straight flow basically remained unaffected. The corresponding detailed measurements of mean and turbulent velocities for a Reynolds number of 31,000 and flowrate ratio of 50% showed that rounding the corner lead to an increase in turbulence in the branch pipe. The increased turbulence diffused momentum more efficiently thus reducing the length of the recirculation by 25% with its width and strength also decreasing in magnitude. The overall effect of the increased dissipation due to turbulence and reduced dissipation due to mean flow irreversibilities in the recirculation was a decrease in the corresponding loss coefficient.*
[DOI: 10.1115/1.2354524]

1 Introduction

Tee junctions are frequently present in industrial systems and water distribution networks where there is the need to separate or merge flows. Disturbances from a condition of straight fully developed flow, such as those created by fittings and accessories, dissipate extra energy [1], which is directly proportional to the intensity of the disturbance. Since 90 deg tee junctions are very disturbing accessories that lead to separated and reverse flows they account for large energy losses if present in large quantities, hence improvements are welcome to reduce the energy bill.

Rounding the corner can help reduce pressure losses, but the separating point becomes dependent on the outlet flowrate ratio, outlet to inlet pipe diameter ratio, pipe roughness, and flow regime. The extent and magnitude of these changes are still poorly understood and documented and constitute the motivation for the present study. Here, the diverging turbulent Newtonian flow in a 90 deg tee junction with sharp corners is experimentally investigated in detail and its flow characteristics are compared with those pertaining to a similar junction with rounded corners.

The amount of available information on 90 deg T-junction flows is rather limited or old and consequently less accurate. The flow is highly complex and three-dimensional and is not accessible to any simplified theoretical analysis. The first series of systematic experimental work in this geometry was carried out in Munich by Vogel [2], who investigated the division and merging of flows in nonsymmetric bifurcations, analyzing the effects of branch pipe diameter and edge radius. Gardel [3,4] included the effects of area ratio, branch angle, and curvature of the junction and derived semi-empirical expressions for the local loss coefficients.

In the 1960s various researchers attempted to justify theoretically the semi-empirical formulas [5]. A theoretical definition of the streamlines and wall pressure distribution in the 90 deg tee was carried out by Iwanami et al. [6] based on the potential flow theory to help understand the mechanisms of pressure loss. They considered the straight pressure loss similar to that in a sudden enlargement whereas the branch pressure loss was modeled as the sum of the loss in a contraction followed by a sudden enlargement. Other investigations in the nineteen sixties and seventies were aimed at confirming and extending results of previous research [7].

More recently, Maia [7] concluded that the traditional pressure field characterization was no longer enough to improve the design of pipe accessories, but required a deeper knowledge of the relationship between flow geometry, pressure field, and flow kinematics. Sierra Espinosa et al. [8,9] investigated round-edge tees and compared a limited set of measurements with simulations by the standard $k-\epsilon$ model, the renormalization group theory (RNG) $k-\epsilon$ model and the standard Reynolds stress (RSM) turbulence models. These models were able to predict the mean flow qualitatively, but the comparisons involving the standard $k-\epsilon$ and RNG models were poor except on the approach flow. Downstream of the T-junction, the RSM could not predict the mean flow as well it overpredicted significantly the extent of the recirculation region in the branch pipe, but it reproduced well the anisotropy of the Reynolds stress tensor. However, careful inspection shows that none of these models did a good job. Recently, Páal et al. [10] used an RSM and the shear stress transport (SST) $k-\omega$ model of Menter [11] to calculate the flow in a 90 deg tee junction with sharp edges; they were able to predict the mean flow reasonably well, but k was significantly under-predicted. The good performance of the SST model was due to its improved ability to deal with separated and rapidly strained flows.

Systematic investigations on the effects of rounding the corner were initially carried out by Boldy [12] and Ito and Imai [13],

[1]Corresponding author.

Contributed by the Fluids Engineering Division of ASME for publication in the JOURNAL OF FLUIDS ENGINEERING. Manuscript received September 9, 2005; final manuscript received May 7, 2006. Assoc. Editor: Timothy J. O'Hern.

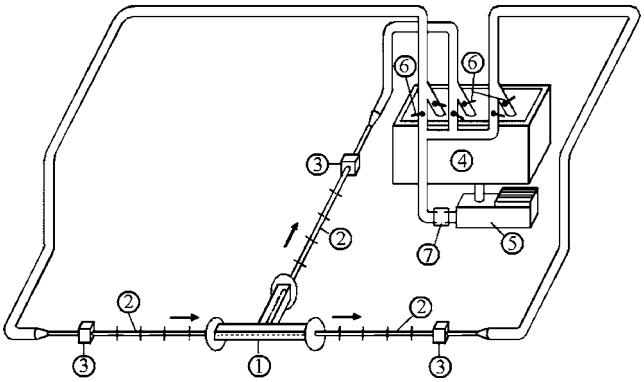

Fig. 1 Schematic representation of the experimental set-up: (1) Tee test section (flow field characterization), (2) pipe test section (pressure field characterization), (3) flowmeter, (4) tank, (5) pump, (6) valve, (7) pulsation dampener

which became the basis of the standard data on energy loss coefficients for tee junctions of the British Hydromechanics Research Association (BHRA) [14].

Today, there is renewed interest on tee junction flows because of the usefulness of diverging flows as separating devices for multi-phase systems found in chemical and power plants [15–17] and the presence of a large number of bifurcations in living organisms even though here the bifurcation angle is less severe [21–25]. In general, in two-phase flow bifurcations there is phase separation with dramatic effects on the pressure differences, and this strongly depends on the geometry, its orientation and type of fluid. Expressions for pressure drop were developed, commonly based on single-phase loss coefficients, taking into account the effects of branch orientation, flow direction (horizontal or vertical, upward, or downward) and its interaction with phase separation [15–17]. More recent research developed split models for annular gas/ liquid separation and measured in detail such flows and in particular the position of the interface [18,19]. Numerical methods have also been developed to deal with gas-liquid and liquid-liquid phase separation in *T*-junctions; Issa and Oliveira [20] used a pressure-volume fraction velocity correction scheme in a conventional seggregated two fluid approach finite volume method.

In living organisms, bifurcations are present in the respiratory and the circulatory system. Here, the approach flow is never fully developed, the pipe is tapered, the flow is time-dependent and the angle of bifurcation is usually well below 90 deg. These investigations are usually in the laminar flow regime [21], very often transient [22], fluids are non-Newtonian [23] and geometries have similarities to true arteries [24], i.e., consecutive junctions in tapered ducts and transient flow. Less often, but equally important, are investigations in the convergent flow as carried out by Ravensbergen et al. [25], amongst others.

The present contribution is aimed at experimentally characterizing and comparing the flows in two similar tees having different edges at the junction: One has a sharp-edged connection between the branch pipe and the main straight pipes whereas the second tee has round edges.

2 Test Rig and Instrumentation

The experiments were carried out in the closed loop rig schematically shown in Fig. 1. The test section was made of two parts: The three 2 m long pipes (pipe test section) and the corresponding extension forming the tee junction test section. The pipe test sections were manufactured from drawn tube with internal diameters of 30.8 mm±45 μm. To reduce optical refraction of laser beams, during the laser-Doppler anemometry measurements, the tee test section was carefully machined from rectangular blocks of acrylic. It is comprised of the bifurcation piece and the three adjoining straight pipes, each of these with 19–26 diameters of overall length for the straight and branch pipes, respectively.

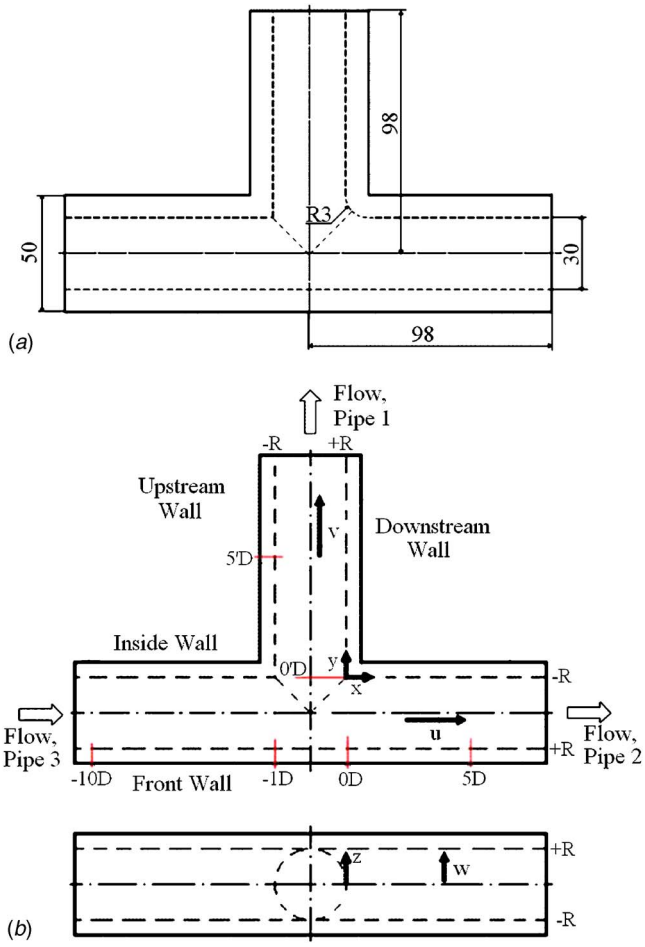

Fig. 2 Test section drawings and co-ordinate system: (*a*) Bifurcation piece: Comparison between sharp-edge tee (left) and rounded-edge tee (right). Dimensions in [mm]; (*b*) coordinate system, position of some diametric measuring planes and terminology.

For the sharp-edge tee bifurcation the pipes were drilled from a single block of acrylic to diameters of 30.1 mm±20 μm. The round-edge tee, which had a ratio of edge radius of curvature to pipe diameter equal to 0.1, was manufactured from two blocks of acrylic using a high precision CAD-CAM system. Then, the two halves were closed and the internal pipe was carefully polished to remove any internal steps/ seams. The internal diameters were checked by means of precision gauges and found to be equal to 30.06 mm±10 μm. Figure 2(*a*) compares the geometries of the sharp (left side) and round-edge (right side) tees, whereas Fig. 2(*b*) shows the coordinate system, the location of some measuring planes and the terminology used throughout this work. The square outer cross-sections of both tees and of the leading pipes minimized refraction of laser beams.

The water flow was continuous and was driven by a volumetric Mohno pump supplied by a constant head tank. A variable speed controller operated the pump and three valves controlled the flow distribution to the two outflow pipes. Pulsation dampeners were also located after the pump to ensure that the flow was continuous. For the detailed velocity measurements the inlet pipe Reynolds number was equal to 32,000 and the flowrate partition to the straight and branch outlet pipes was 50%/50%. For the pressure

measurements the inlet Reynolds number varied from 5000 to 32,000 while the volumetric flowrate ratio Q_1/Q_3 was varied from 0 to 1 (branch flow rate over inlet flow rate).

The flow rates were monitored by three magnetic flowmeters, one in each pipe, and the temperature of the water was monitored by means of a PTC100 sensor located in the open tank. The water temperature variation during each test run was within the sensor uncertainty of ±0.5 °C, because of the large volume of water in the rig, but varied along the year. Its influence on the viscosity was taken into account to maintain the inlet flow conditions. The 95% confidence level uncertainties of the flowrate measurements varied between 2.5% and 0.6% at low and high flowrates, respectively.

Pressure measurements were carried out along the pipes to obtain the loss coefficients for the straight and branched flows. On each pipe there were seven measuring planes in the 2 m nearer to the bifurcation and in each of these measuring planes there were four pressure taps uniformly distributed around the perimeter of the pipe and connected to each other. The pressure from each pressure section was connected to a differential pressure transducer via a valve switchboard. The differential pressure transducer was a Rosemount, model 3051C, and was interfaced with a computer via an AD converter. The uncertainties of the pressure differences were of 6.7% at Re=15,000, decreasing to 1.2% at Re =40,000. These uncertainties were estimated following the square root of the sum of squares procedure explained in detail in Coleman and Steele [26]. Here, the total relative uncertainty ($E_{\Delta p}/\Delta p$) was calculated from the total systematic ($B_{\Delta p}$) and precision ($P_{\Delta p}$) uncertainties following Eq. (1):

$$\frac{E_{\Delta p}}{\Delta p} = \sqrt{\left(\frac{B_{\Delta p}}{\Delta p}\right)^2 + \left(\frac{P_{\Delta p}}{\Delta p}\right)^2} \tag{1}$$

The total systematic uncertainties included contributions from the fossilized uncertainty of the transducer, its resolution and the fossilized total uncertainty from the calibration procedure. During calibration, the pressure transducer ports could be switched to measure the pressure difference between two independently filled water columns, their heights measured by electrodes positioned using two verniers. The precision uncertainty was given by

$$P_{\Delta p} = t\frac{S_{\Delta p}}{\sqrt{N}} \tag{2}$$

where $S_{\Delta p}$ is the standard deviation of the sample of N readings (N=1000 pressure readings) and t=2 since the sample was larger than 10 (as recommended by Coleman and Steele [26]). More details of the uncertainty analysis are given in Costa [27].

Mean and turbulent velocity measurements in the pipes and tees were carried out by means of laser-Doppler anemometry. The LDA used was a miniaturized fiber optics system from INVENT, model DFLDA, similar to that described in detail by Stieglmeier and Tropea [28], with a 120 mm front lens mounted onto the 30 mm diameter probe (probe S30). Scattered light was collected by a photodiode in the forward- and backscatter modes, depending on optical access. In particular, in the T-junction test section the measurements could only be done in backscatter mode, because of the size of the supports of the ducts and the bulky receiving optical unit. The main characteristics of the anemometer are listed in Table 1.

The signal from the photodiode was processed by a TSI 1990 C counter, which contained the filters required to remove the pedestal. It operated in the single measurement per burst mode, frequency validation was set at 1% and 16 signal cycles were used for each valid measurement. The counter was interfaced with a computer via a DOSTEK 1400A card, which provided the statistical quantities. To measure the three components of the velocity vector with a 1D LDA we followed standard procedures. For all velocity components Snell's law [29] was taken into account to quantify the effects of curvature of the pipe walls in positioning the LDA measuring volume, in the value of the LDA conversion factors and in determining the orientation of the velocity component being measured at the control volume. For the streamwise velocity the plane of laser beams was diametric and the control volume was traversed radially along the laser light direction from wall to wall. To measure the tangential and radial velocity components the plane containing the laser beams was perpendicular to the pipe axis. The control volume was traversed radially along the laser light direction to measure the tangential velocity. Radial traversing the control volume along the direction perpendicular to the direction of the LDA measured a combination of the radial and tangential velocity components that required post-processing.

Table 1 Main characteristics of the laser-Doppler system (more characteristics in Table 1 of Stieglmeier and Tropea [28])

Laser wavelength	820 nm
Laser power	100 mW
Laser diameter	3.5 mm
Measured half-angle of beams in air	3.81 deg
Size of measuring volume in water (e^{-2})	
minor axis	37 μm
major axis	550 μm
Fringe spacing in air	6.31 μm
Frequency shift	1.0 MHz

The maximum uncertainties in the streamwise mean and rms velocities at a 95% confidence level are of 0.9% and 2.5% in low turbulence regions and of 1.5% and 5.5% in high turbulence regions close to walls, respectively. The uncertainty in the measurements of the cross-stream mean and rms velocity components is 1.4% and 6.0% in low and high turbulence regions, respectively. To estimate the uncertainties in the LDA measurements we followed Durst et al. [30] and Albrecht et al. [29], and took into account the specificities of the system used, which are described in detail by Stieglmeier and Tropea [28]. The total uncertainties of the mean and rms velocities were estimated on the basis of following contributions: Statistics (5000 data samples), clock accuracy and number of fringe effects, averaging process, beam alignment relative to geometry, effect of small scale fluctuations, and velocity gradient broadening. No corrections to gradient broadening were applied to the measured data and the broadening due to the number of fringes was always well below 0.4%, because the number of static fringes was six, the number of periods in signal processing was 16, the fringe spacing was 6.31 μm, the counter used had a clock frequency of 500 MHz, the shift frequency was 1 MHz, and the velocities measured corresponded to Doppler frequencies less than 0.3 MHz. Measurements could be performed to within 200 μm of the wall.

The anemometer was mounted on a milling machine with movement in the three coordinate directions and the positional uncertainty was ±100 μm in all three directions.

3 Experimental Results and Discussion

3.1 Sharp-Edge Tee

3.1.1 Pressure-Field Characterization. According to the flow configuration of Fig. 2, the energy equations for the two flow paths are given by

$$p_3 + \frac{1}{2}\alpha_3\rho U_3^2 = p_1 + \frac{1}{2}\alpha_1\rho U_1^2 + f_3\frac{L_3}{D_3}\rho\frac{U_3^2}{2} + f_1\frac{L_1}{D_1}\rho\frac{U_1^2}{2} + \Delta p_{3-1} \tag{3}$$

$$p_3 + \frac{1}{2}\alpha_3 \rho U_3^2 = p_2 + \frac{1}{2}\alpha_2 \rho U_2^2 + f_3 \frac{L_3}{D_3}\rho \frac{U_3^2}{2} + f_2 \frac{L_2}{D_2}\rho \frac{U_2^2}{2} + \Delta p_{3-2} \tag{4}$$

for the branched and the straight flows, respectively. The subscripts 1–3 refer to the branch pipe, the straight outlet pipe, and the inlet pipe, respectively. The static pressure is p, U is the bulk velocity (in the absence of subscript U represents U_3), ρ is the density of the fluid, f is Darcy's friction coefficient for fully developed flow in a pipe of diameter D, and the length is L. The length of a pipe is measured from the position of the pressure tap to the intersection of the three pipes. The pressure losses associated with the tee are given by Δp_{3-j} in the trajectory from pipe 3 to pipe j. The energy shape factors (α) are taken to be 1, the usual engineering practice in calculations when the flow is turbulent. From the pressure measurements taken along the straight pipes, in regions of fully developed flow, the values of the Darcy friction factors were determined for each pipe. The pressure losses in the tee were subsequently evaluated from the measured pressure differences and application of Eqs. (3) and (4). The corresponding local loss coefficients are defined as

$$K_{31} \equiv \frac{\Delta p_{3-1}}{\frac{1}{2}\rho U_3^2} \tag{5}$$

$$K_{32} \equiv \frac{\Delta p_{3-2}}{\frac{1}{2}\rho U_3^2} \tag{6}$$

It is important to note at this stage that the inlet Reynolds numbers (Re_3) of the measured flows are low for a turbulent flow. In contrast, some data from the literature shown in Figs. 3–5, pertain to high Reynolds number flows where the loss coefficients are already independent of the Reynolds number.

For these experimental conditions, Figs. 3 and 4 present the variations of coefficients K_{31} and K_{32} with inlet pipe Reynolds number and flow rate partition and compare the measurements with data from the literature. Looking first at our measurements in Figs. 3(a) and 4(a), it is clear that at high Reynolds numbers both coefficients are independent of Re, whereas at low Reynolds numbers K_{31} decreases and K_{32} increases with Re. The variation of both coefficients with flow rate ratio, shown in Figs. 3(b) and 4(b), is nonmonotonic, with minimum values of K_{31} at $Q_1/Q_3 \cong 0.4$ and of K_{32} at $Q_1/Q_3 \cong 0.2$. The variations in the magnitude of K_{32} in relation to Re and Q_1/Q_3 are stronger than the variations in K_{31}, but only in relative terms.

Comparisons with the literature are shown in Figs. 3(b) and 4(b); they are reasonably good considering the experimental uncertainties, differences in Reynolds number, variations in the geometry, and in the inlet flow conditions. In particular, for our measurements at a Reynolds number of 32,000 and a flow rate ratio of 50%, the values of K_{31} and K_{32} are equal to 0.86 and 0.036, respectively. This is the flow condition at which the mean and turbulent velocity fields, presented in the next two subsections, were investigated in detail.

3.1.2 Inlet Flow Field. We start by presenting radial profiles of the mean and rms velocities in the inlet pipe. In Fig. 5(a) wall coordinates are used whereas Figs. 5(b)–5(d) and 6 show plots in physical coordinates. In particular, data for two upstream sections are presented (−10 and −5 D) and in Fig. 5 they are also compared with classical data from the literature [31–33]. More recent literature data [34,35] concentrate on the near wall region and pertain to very low flow Reynolds numbers, and they also agree with the classical data away from the near wall region. Given our set-up and LDA system, the classical data are adequate for these comparisons. The axial mean velocity in wall coordinates in Fig. 5(a) compares well with the log-law and the experimental data.

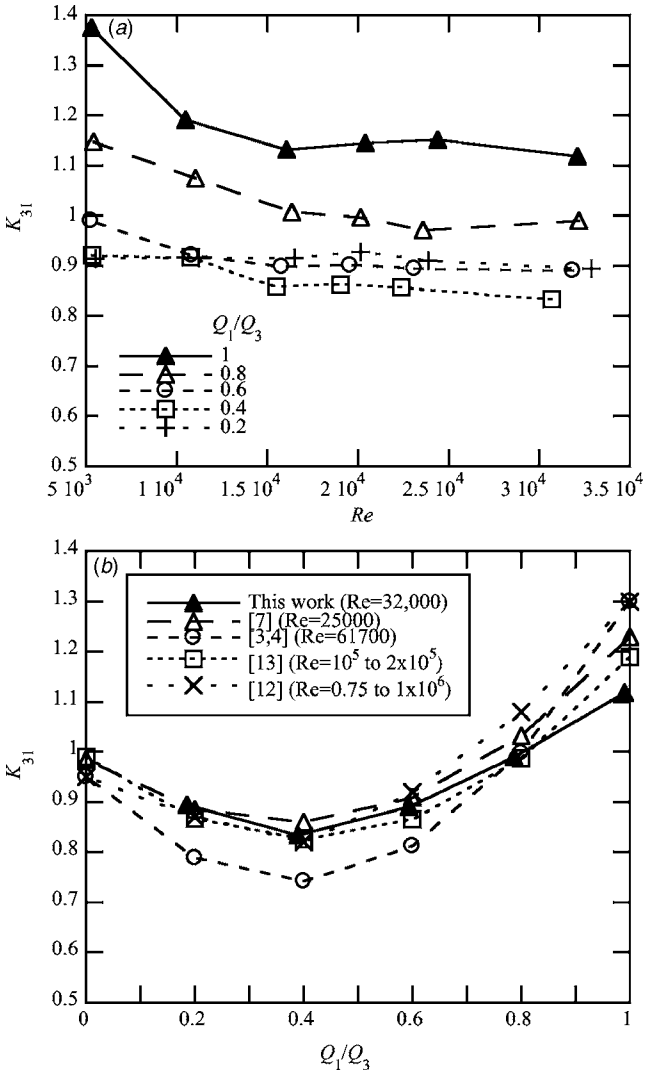

Fig. 3 Variation of the local loss coefficient K_{31} in a sharp edge 90 deg tee: (a) Effect of Reynolds number and flow rate ratio; (b) comparison with literature

The corresponding data in physical coordinates shown in Fig. 6, at a Reynolds number of 35,000, are also consistent with the literature and the ratio between the centerline and bulk velocities, slightly exceeding 1.2, was also expected.

In terms of turbulence data, the profiles of the rms velocities are also in good agreement with the literature. Near the wall the measured data exceed the literature values, because they were not corrected for mean gradient broadening effects. In conclusion, the inlet flow is well developed upstream the bifurcation both in terms of mean and turbulent flow.

3.1.3 Mean Flow Field. Figure 7 presents radial profiles of the axial mean and rms velocities inside the bifurcation region to illustrate the distortion of the flow at the inlet (−1 D) and inside (−0.5 D) the bifurcation. Here and elsewhere, the data were normalized by the inlet pipe bulk velocity ($U=U_3$). The distortion in the axial velocity is maintained between −1 and −0.5 D, while part of the fluid goes into the branch pipe. The slightly increased turbulence at −0.5 D could be associated with the small flow deceleration in the region. The flow remains symmetric in the z-direction as we can see from the profile of the axial mean velocity taken vertically at −1 D.

The mean flow is best understood with the vector plot of the mean velocity in the x-y horizontal diametric plane of Fig. 8. In

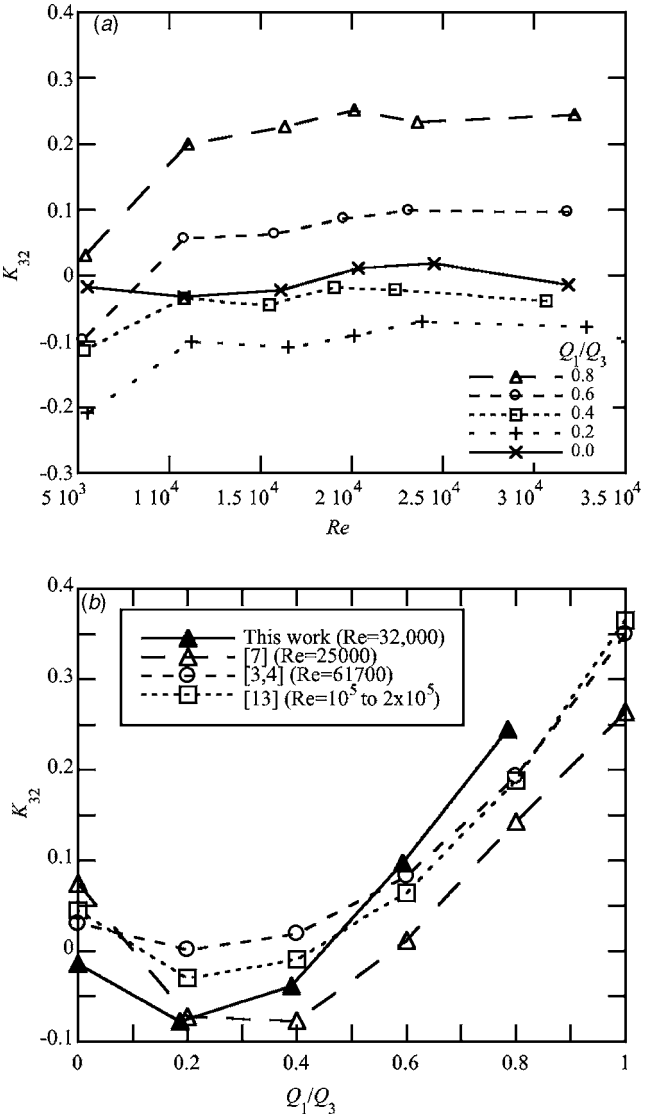

Fig. 4 Variation of the local loss coefficient K_{32} in a sharp edge 90 deg tee: (*a*) Effect of Reynolds number and flow rate ratio; (*b*) comparison with literature

the inlet and main outlet pipes u is the streamwise velocity and v is the cross-stream velocity; in the branch pipe the role of these two velocity components change. In referring to measuring stations, a prime designates the branch pipe, and negative values identify stations inside the bifurcating regions (cf. Fig. 2: 0 D and 0′ D represent the entrance to the outlet and branch pipes, respectively).

On approaching the beginning of the bifurcation (−1.0 D) the flow in the inlet pipe deviates towards the inside wall. At the middle of the bifurcation (−0.5 D) the maximum normalized streamwise velocity has dropped only to about 0.9, indicating that in the first half of the junction the main flow does not deviate significantly towards the side branch (see also Fig. 7), because the recirculation zone at the edge of the upstream wall of the branch pipe blocks the passage of fluid, which goes into the branch pipe only at the downstream half of the junction. This can also be seen in the radial profiles of the streamwise velocity in the branch pipe of Fig. 9. Here, it is clear that the recirculation bubble becomes wider than the radius of the branch pipe, starting from the upstream wall (cf. profiles from 0.25′ to 1.5′ D).

The recirculation bubble in the branch pipe is about 2.0′ D long, its width remains fairly constant and the maximum streamwise velocities occur between 1.1′ and 1.5′ D. The shape of the recirculating region at its end is rather strange; at 2.0′ D the flow near the upstream wall is already positive but there is still a small negative velocity near the pipe axis showing that the recirculation has detached from the wall to form a bubble in the center of the pipe. This pattern is similar to that measured by Maia [7] under laminar flow conditions, even though here the flow is turbulent. Close inspection of the vectors inside the recirculating region show also that the fluid is moving away from the wall, and continuity requires that an inflow into the wall region must take place. This leads to a strong 3D flow with the w velocity component feeding fluid into this region from above and below the horizontal diametric plane. Some measurements of w were carried out in this region and confirm this finding as shown in Fig. 10. Here, "radial" profiles of the vertical velocity (w) measured 10 mm above and 10 mm below the diametric horizontal plane are plotted. Negative values of r correspond to the vicinity of the upstream wall where strong jets are seen feeding fluid into the recirculation. Velocities w are positive below the diametric plane and vice versa.

Because the flow deviation into the branch mostly takes place near the end of the bifurcation, the shape of the streamwise velocity profile at the beginning of the straight outlet pipe (plane 0.0 D), shown in Fig. 11 (circles), is almost symmetric. However, downstream of the entrance to the outlet straight pipe the streamwise velocity profiles become quickly distorted due to the large values of v/U in combination with the sudden appearance of the wall, leading to profiles of u/U strongly skewed towards the inside wall. Flow redevelopment in the straight outlet pipe takes a while to be noticed: At 2.0 D the fluid is already accelerating at the outside wall but at 5.0 D the profile is still distorted.

Cross-stream velocities in the horizontal direction in the main and branch pipes (v and u, respectively) are very low everywhere (not exceeding 5% of inlet bulk velocity) except at the entrance to the pipes where the flow tends to be aligned at 45 deg relative to both the x and y axis and attains values of 15% of the inlet bulk velocity.

In the vertical plane the flow remains symmetric as can be assessed by some radial profiles of the streamwise velocity taken in a vertical cross-stream direction and plotted as crosses in Fig. 11. Compared with the horizontal profiles of Fig. 11 the evolution of u/U is quite different. While the velocity at the center of the pipe quickly decreases on going downstream, near the upper and bottom walls it increases and the profile remains symmetric, an indication of the strong three-dimensional character of the flow. In contrast, in the horizontal plane the streamwise velocity profiles are asymmetric and the peak velocity is observed to remain near the inside wall for a long time (cf. circles in Fig. 11). It is also worth mentioning that for this flowrate ratio (50%) no flow separation was observed in the main outlet pipe.

3.1.4 Turbulent Flow Field. Figures 12–14 present profiles of the normalized u' and v' in the bifurcation, the straight outlet pipe and branch pipe of the sharp-edge tee, respectively.

Starting in the bifurcation, Fig. 12 shows that the turbulence increases as the fluid moves from the inlet pipe towards the exit, but the larger increase in u'/U is seen near the front wall, probably a consequence of production of $\overline{u'^2}$ by normal rate of strain-normal Reynolds stress interaction (first term on the right-hand-side (RHS) of Eq. (7)), as suggested by Hinze [36]. In fact, on entering the bifurcation the mean flow is already deviating towards the inside wall, because of the imminent change in direction of 50% of the fluid that goes into the branch pipe. The consequence is a fluid deceleration in the front wall region of the bifurcation due to depletion of fluid ($\partial u/\partial x < 0$) leading to a positive first term on the RHS of Eq. (7)

$$\text{Production of } \overline{u'^2} = -\overline{u'^2}\frac{\partial u}{\partial x} - \overline{u'v'}\frac{\partial u}{\partial y} - \overline{u'w'}\frac{\partial u}{\partial z} \qquad (7)$$

From 0.0 to 1.0 D, in the straight outlet pipe, the horizontal

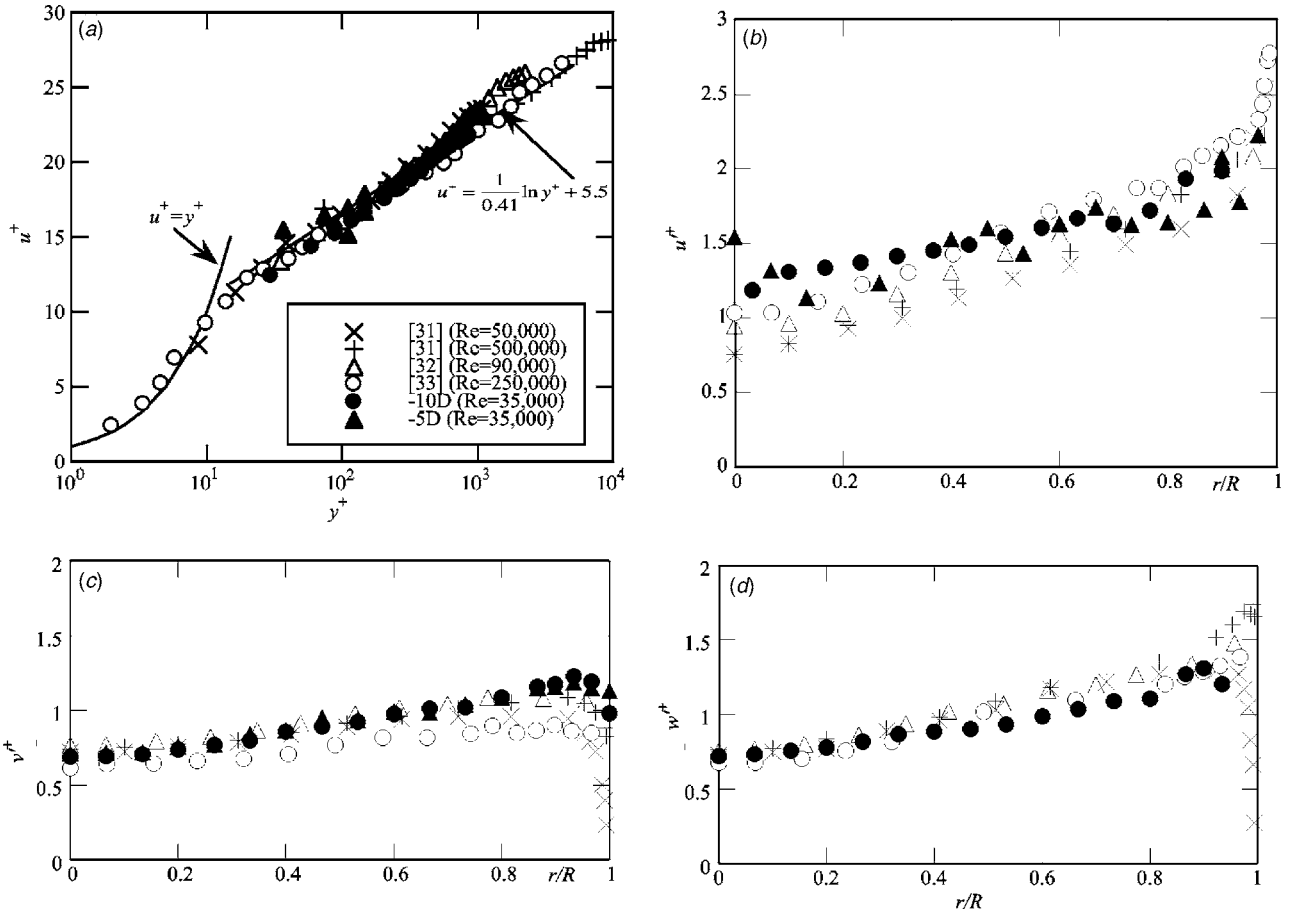

Fig. 5 Comparison between the literature and measured velocity profiles upstream of the tee junction (–10 and –5 D): (*a*) Axial velocity (in wall coordinates); (*b*) axial rms velocity; (*c*) radial rms velocity; (*d*) tangential rms velocity

profiles in Fig. 13(*a*) show that u'/U decreases in the front wall region ($r>0$) and increases in the inside wall region ($r<0$). In the former region the boundary layer is weak (circles in Fig. 11 show a low shear rate), because this region has been previously depleted of fluid and so the turbulence production by shear velocity gradient and shear Reynolds stress interaction (the second term on the RHS of Eq. (7)) will be smaller than at the equivalent region in the inlet pipe. Also, fluid with lower turbulence is being advected from the inside wall region of the outlet pipe into the front wall region, thus decreasing turbulence by fluid mixing as

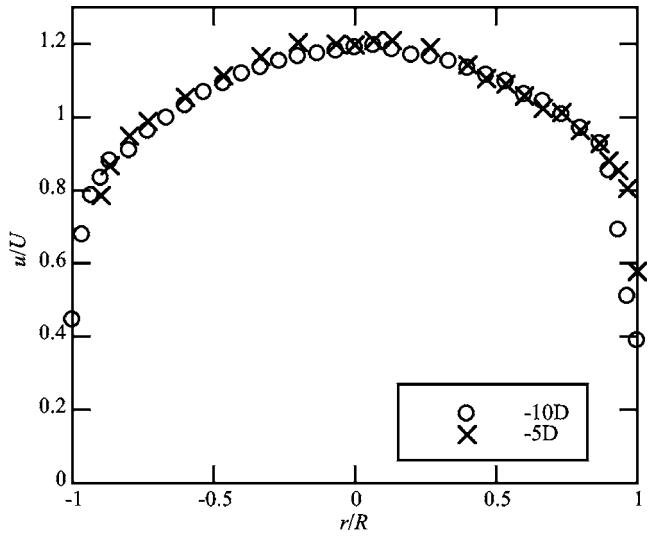

Fig. 6 Radial profiles of the normalized axial mean flow upstream of the tee junction (–10 and –5 D) at Re=35,000

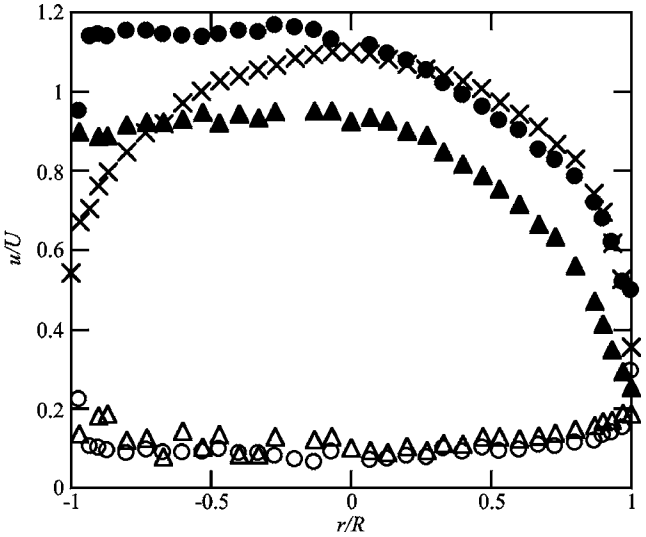

Fig. 7 Radial profiles of mean (closed symbols) and rms axial velocity (open symbols) in the bifurcation region of the sharp-edge tee: –1 D (○), –0.5 D (△); vertical cross-stream profile at –1 D (×)

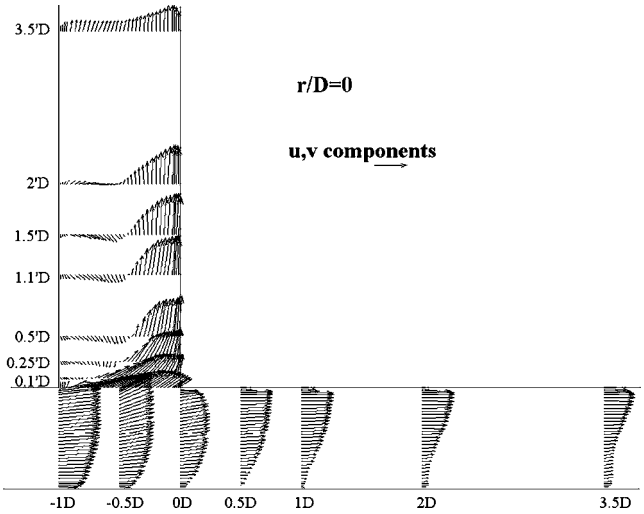

Fig. 8 Vector plot of the mean velocity in the horizontal diametric plane *x-y* of the bifurcation of the sharp-edge tee for Re=32,000 and $Q_1/Q_3=50\%$. The scale vector corresponds to $u/U=1$.

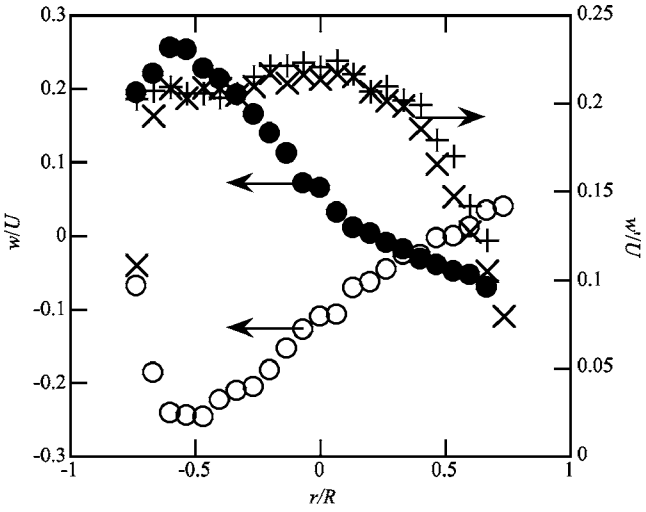

Fig. 10 "Radial" profiles of w/U (○, ●) and w'/U (×, +) measured 10 mm above (○, ×) and 10 mm below (●, +) the diametric horizontal plane at 2.0′ D for the sharp edge tee flow at Re=32,000 and $Q_1/Q_3=50\%$

well as by fluid acceleration in the front wall region ($\partial u/\partial x>0$ implies $-\overline{u'^2}\partial u/\partial x<0$ in Eq. (7)). Conversely, in the inside wall region turbulence increases for the opposite reasons. Since we cannot measure the Reynolds shear stresses in a pipe with a 1D LDA system (unless a refractive index matching technique is used), the two shear contributions to Eq. (7) could not be quantified and the above interpretation is merely qualitative, but nevertheless it is in agreement with the specialized literature [36,37].

In the outlet pipe, the profiles of rms velocities are symmetric along the vertical cross-stream direction and also show decreasing turbulence near the walls on moving downstream.

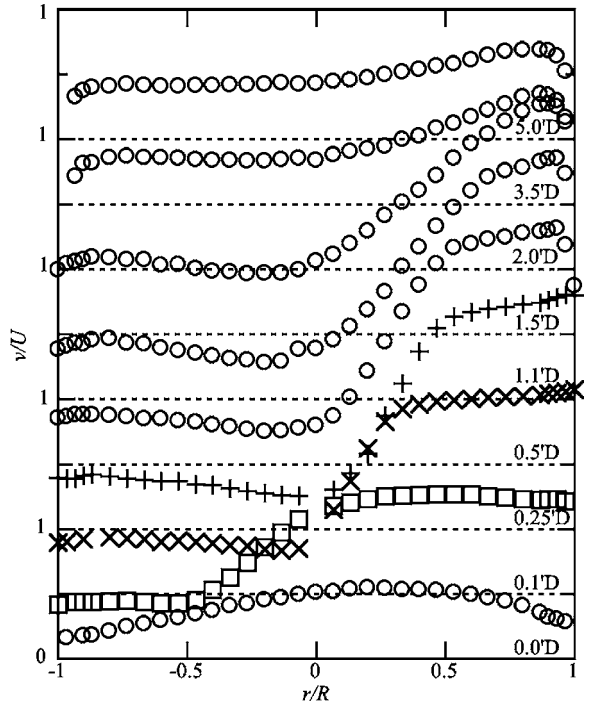

Fig. 9 Radial profiles of streamwise velocity in the branch pipe of the sharp-edge tee for Re=32,000 and $Q_1/Q_3=50\%$

To analyze the turbulence in the branch pipe it is convenient to write down the expression for the production of the corresponding streamwise normal Reynolds stress, in Eq. (8)

$$\text{Production of } -\overline{v'^2} = -\overline{u'v'}\frac{\partial v}{\partial x} - \overline{v'^2}\frac{\partial v}{\partial y} - \overline{v'w'}\frac{\partial v}{\partial z} \qquad (8)$$

As seen in Fig. 9, there is a very strong shear layer in the center of the branch pipe, between the attached recirculating region and the jet along the downstream wall of the tee. Here, there will be production of $\overline{v'^2}$ by shear interactions (first term on the right-

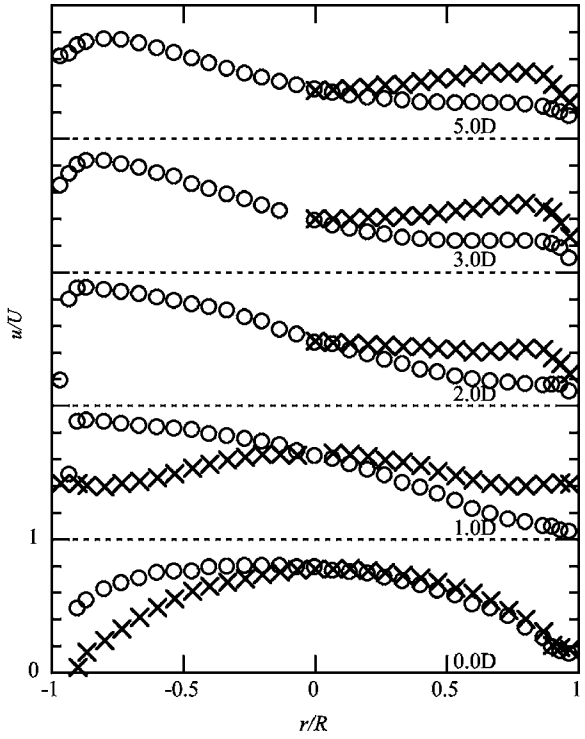

Fig. 11 Radial profiles of streamwise velocity in the outlet pipe of sharp edge tee for Re=32,000 and $Q_1/Q_3=50\%$: ○—measurements in horizontal plane; ×—measurements in vertical plane (full and half profiles)

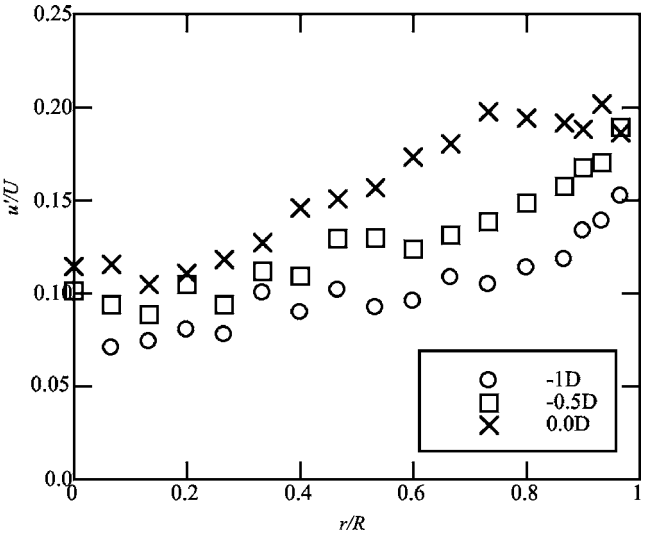

Fig. 12 Radial profiles of u'/U in the junction region of the sharp-edge tee for Re=32,000 and $Q_1/Q_3=50\%$, measured between the axis and the front wall

hand-side (RHS) of Eq. (8)) and consequently there is a maximum in the profiles of v'/U near the pipe center (at $r/R \approx -0.25$, +0.1, and +0.2 in stations $x=0.1'$ D, $0.25'$ D, $0.5'$ D, and until $1.5'$ D) shown in the horizontal radial plots in Fig. 14(*a*).

Large streamwise mean velocity gradients $\partial v/\partial y$ are found along the downstream wall of the branch pipe due to the strong wall jet (initially positive (fluid acceleration), later negative (fluid deceleration)). This will contribute to initially decrease (at $r/R \approx 1$, from stations $x=0.0'-0.5'$ D), and later increase (at $r/R \approx 1$, for stations $x \geq 1.1'$ D) the values of v' in this region via the second term on the RHS of Eq. (8). There is also an increase in turbulence within the recirculation (near the wall for $r/R<0$), but here there will also certainly be important contributions from turbulent diffusion and advection. The advective transport of turbulence into this recirculating region includes contributions of fluid from above and below the horizontal diametric plane, which has turbulence of the order of $0.2U$ (cf. w' data above/below diametric plane in Fig. 10). This level of turbulence is in excess of what is found at the early stages of the recirculation (see profiles of v' at $0.0'$ to $0.25'$ D in Fig. 14(*a*)). Further downstream, all turbulence components decrease as the flow starts to redevelop.

Horizontal radial traverses of u', not shown here for conciseness, also show the turbulence increase in the center of the branch pipe when moving from $0.0'$ to $1.1'$ D, followed by a decrease, but near the walls u' always remains low, even inside the recirculation. Vertical cross-stream profiles of v' and u' are plotted in Figs. 14(*a*) and 14(*b*), respectively, and also show well the increase in turbulence in the center of the branch pipe up to $1.1'$ D, associated with the presence of the shear layer bordering the recirculation, and its decrease on going further downstream. Note that in the branch pipe the variations of v' are more intense because this is the velocity component that is being directly produced (for fully developed flow in the branch pipe, production of $\overline{u'^2}$ is zero and this normal Reynolds stress acquires its energy via pressure strain redistribution).

3.2 Round-Edge Tee: Comparison With the Sharp Edge

3.2.1 Pressure Field Characterization. The variations of the local loss coefficients for the straigth (K_{32}) and branched pipes (K_{31}) are presented in Figs. 15 and 16 as a function of the inlet Reynolds number and flowrate ratio. The figures include data from the literature and show variations which are similar to those

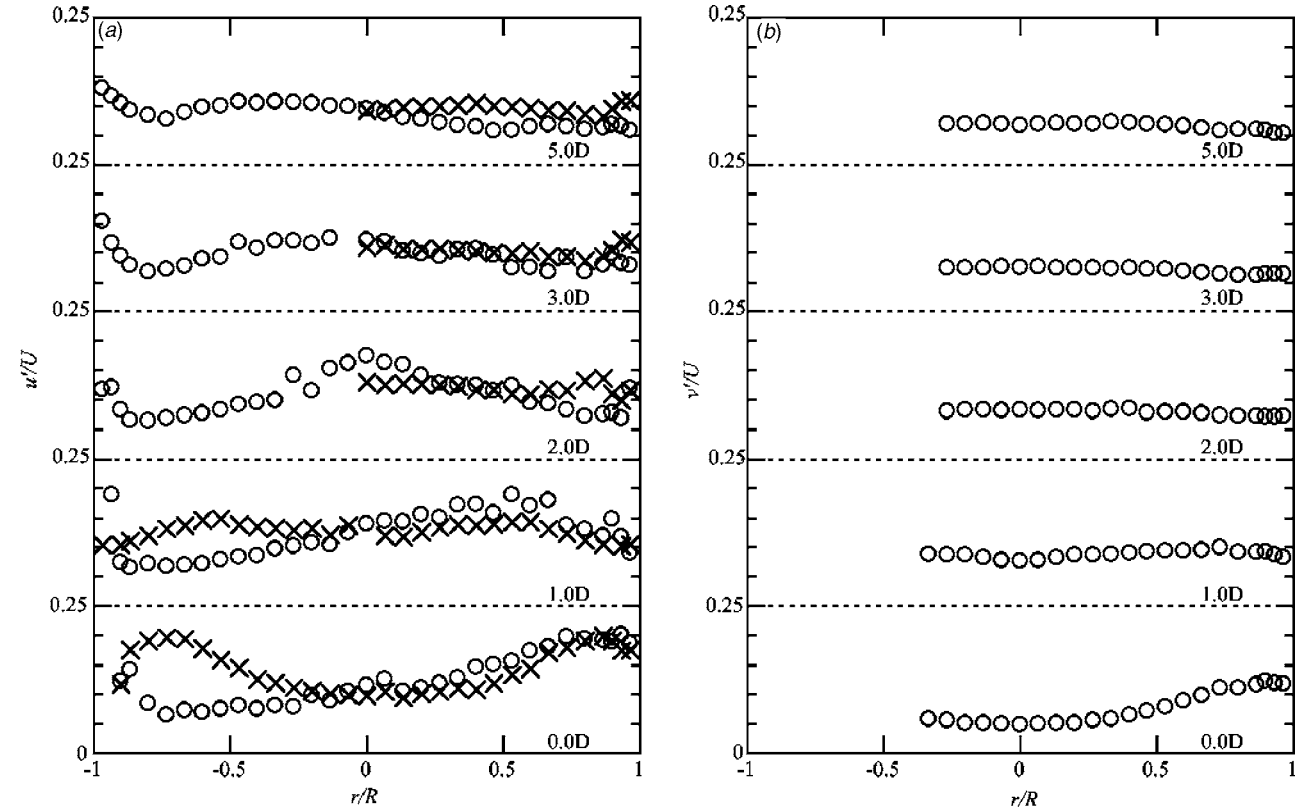

Fig. 13 Radial profiles of u'/U and v'/U in the outlet straight pipe of the sharp-edge tee for Re=32,000 and $Q_1/Q_3=50\%$. (*a*) u'/U (◯: Horizontal cross-stream profile; ×: Vertical cross-stream profile); (*b*) v'/U (vertical cross-stream profile).

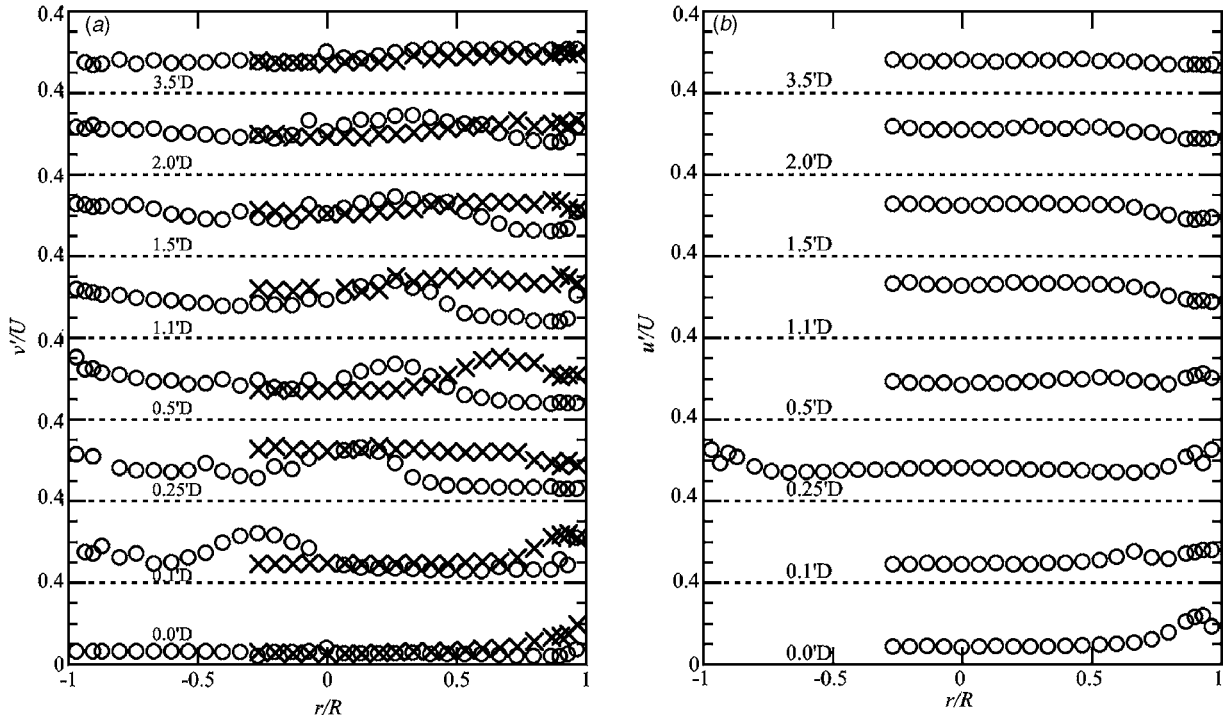

Fig. 14 Radial profiles of v'/U and u'/U in the branch pipe of the sharp-edge tee for Re=32,000 and Q_1/Q_3=50%. (*a*) v'/U (○—horizontal measurement; ×—vertical measurement); (b) u'/U (vertical cross-stream profile).

seen in Figs. 3 and 4 for the sharp edge tee, but now taking lower numerical values especially for coefficient K_{31} on account of the less severe conditions due to a round edge.

Careful inspection of these figures and direct comparison between Figs. 3 and 15 show that rounding the corner reduces the pressure loss for the branched flow especially at high flow rate ratios, i.e., when a higher proportion of fluid is forced to go through the branch pipe: For $Q_1/Q_3=1$ and Re$>$15,000 there is a reduction in K_{31} from about 1.1 to 0.9, whereas at $Q_1/Q_3=0.4$, when K_{31} goes through a minimum, the decrease is from 0.85 to about 0.75 and at $Q_1/Q_3=0.2$ the difference is even smaller. This agrees with the literature, although more pronounced effects may be found there for more rounded corners. As a matter of fact our measurements pertain to a less rounded corner than those of Maia [7], but correspond to Reynolds numbers of the same magnitude (27,000 against our 30,000) leading to higher values for the loss coefficients: At $Q_1/Q_3=0.8$ we measured $K_{31}\approx 0.8$ against a value of around 0.52 measured by Maia [7].

At low Reynolds number, the variation of K_{32} with the Reynolds number is opposite to that seen for the sharp tee: Whereas K_{32} increases with Re for the sharp tee, it decreases for the round tee. At high Reynolds numbers the straight flow is basically unperturbed by the shape of the corner and the differences in K_{32} are within experimental uncertainty, as shown by a direct comparison between Figs. 4(*b*) and 16(*b*) for Re$\approx$31,000. However, as the Reynolds number is reduced the pressure loss becomes lower for the sharp edge tee, i.e., there is no advantage in rounding the corner as far as K_{32} is concerned. This has also been seen by Maia [7] at a Reynolds number of 26,000 (with a smoother edge curvature), who also stated that the curves for K_{32} in the literature are considered universal, i.e., independent of R/D, when the Reynolds number is high.

The comparison between the round and sharp-edge tees should not be made simply by looking at individual flow paths and loss coefficients. Rounding the corner affects differently the two local loss coefficients, therefore, it is advantageous to compare the performance of both tees by looking at the total energy loss. This is achieved defining a total loss coefficient (K_D) accounting for all the energy dissipated in the tee as

$$K_D=\frac{Q_1}{Q_3}K_{31}+\frac{Q_2}{Q_3}K_{32} \tag{9}$$

For both tees, the variation of K_D with the flow rate ratio at a constant Reynolds number of around 31,000 is shown in Fig. 17 from where it becomes clear the advantage of the round-edge tee. At low flow rate ratios there is basically no difference, but for Q_1/Q_3 of around 0.4 the difference is already of 10% and rising to 20% at higher flow partitions.

3.2.2 Mean Flow Field. The general features of the mean flow are similar to those seen with the sharp edge tee, the few differences requiring a detailed inspection of the mean flow field. Starting at the bifurcation region, profiles of the stream-wise mean velocity at −1 and −0.5 D are plotted in Fig. 18; at the inside wall region the velocities are consistently higher by 5–10% than for the sharp edge tee (compare with Fig. 7), because the flow enters more easily into the branch pipe when the corner is round. Detailed inspection of the vector plot in Fig. 19 show also important differences relative to the flow in the sharp edge tee inside the branch pipe of Fig. 8: For the round tee at 1.5′ D the velocity vectors inside the recirculation are less negative whereas at 2.0′ D they are already positive, suggesting a shorter recirculation than for the sharp tee.

The radial profiles of the streamwise velocity inside the branch pipe plotted in Fig. 20 are directly comparable to those for the sharp tee in Fig. 9. They confirm that for the round tee the attached recirculation ends at around 1.5′ D (for the sharp tee that happens at around 2.0′ D), even though there is still a recirculation separated from the wall in the center of the pipe, the velocity in the downstream wall jet peaks at 1.1′ D, rather than at 1.5′ D as in the sharp tee, and the velocities within the recirculation are less negative than for the sharp tee. Flow redevelopment is also

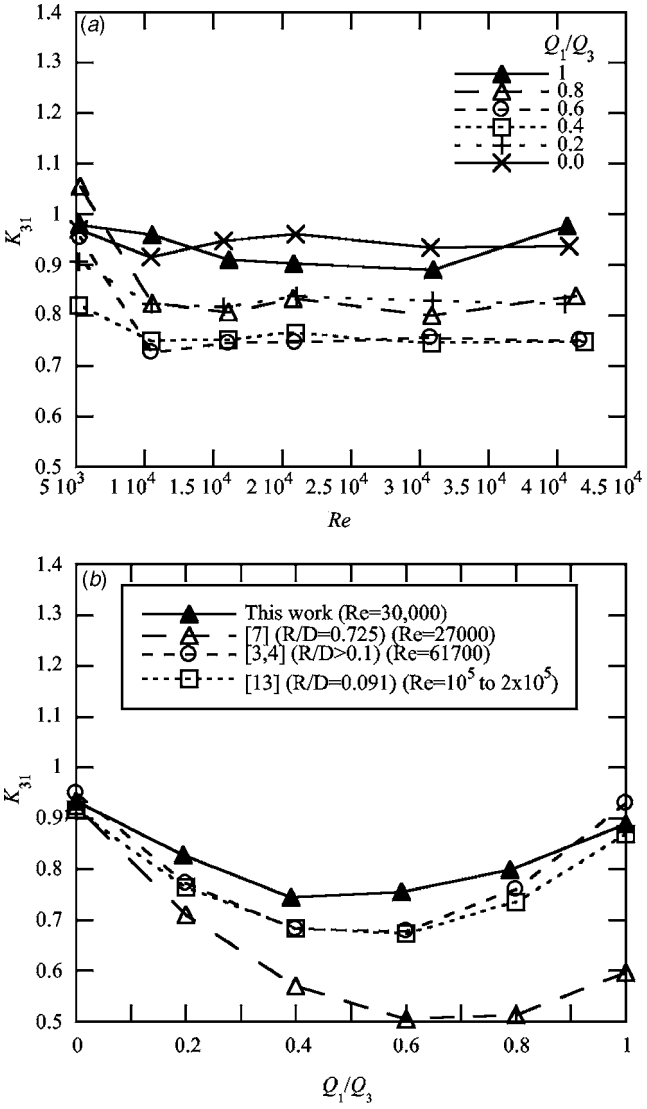

Fig. 15 Variation of the local loss coefficient K_{31} in a rounded edge (R/D=0.1) 90 deg tee: (*a*) Effect of Reynolds number and flow rate ratio; (*b*) comparison with literature

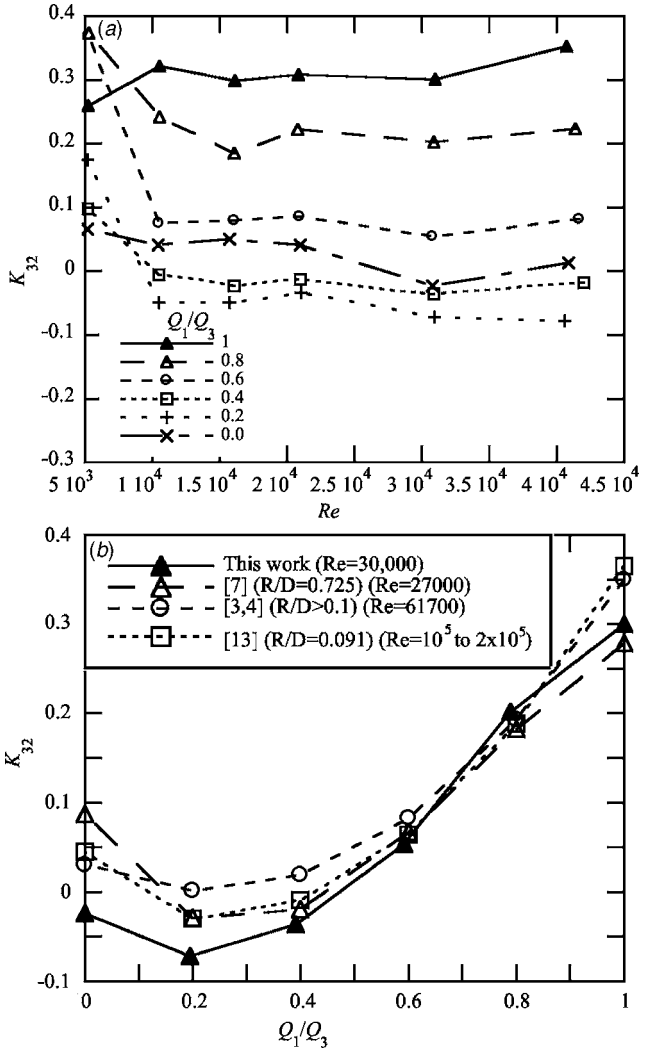

Fig. 16 Variation of the local loss coefficient K_{32} in a rounded edge (R/D=0.1) 90 deg tee: (*a*) Effect of Reynolds number and flow rate ratio; (*b*) comparison with literature

quicker with the round tee (cf. the profile at $5.0'$ D which is almost flat), i.e., the main effect of rounding the edge is to reduce the length, width, and strength of the separated flow region. A decrease in the recirculation length has also been observed in the limited experiments of Sierra-Espinosa et al. [9] in a similar flow situation, but with a different edge curvature, and these findings are consistent with the lower energy loss measured for the flow going into the branch (lower K_{31}) when the corner is rounded.

Regarding the flow in the straight outlet pipe, the radial profiles of streamline mean velocity in Fig. 21 pertain to the round-edge tee and are to be compared with the corresponding profiles for the sharp tee of Fig. 11. The velocity profiles are almost identical and differences seen in profiles of the cross-stream velocity (not shown) are within experimental uncertainty. As already mentioned, the flow is symmetric relative to the mid-plane of the tee and this is well shown in the radial profiles of streamwise velocity taken vertically and plotted as crosses in Fig. 21.

3.2.3 Turbulent Flow Field. For the round tee the profiles of u'/U and v'/U are always higher than for the sharp tee, but in varying degrees. Inside the bifurcation region the differences are insignificant since they are within experimental uncertainty. For the straight outlet pipe the turbulence data are plotted in Fig. 22

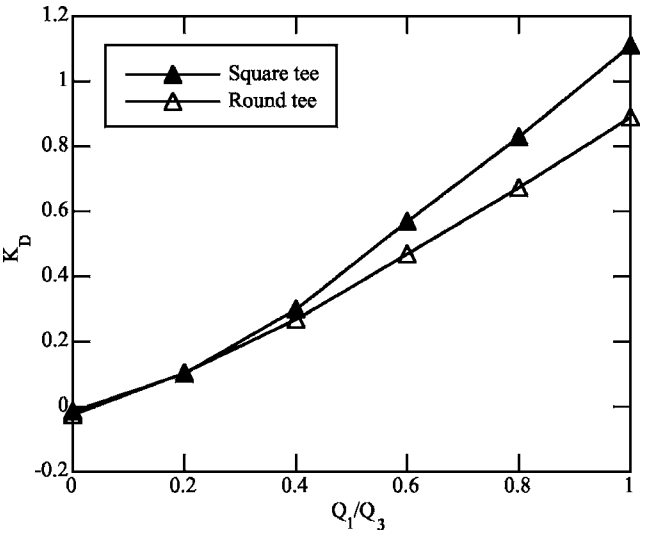

Fig. 17 Comparison between the sharp and round corner tees in terms of total energy loss for Re≈31,000

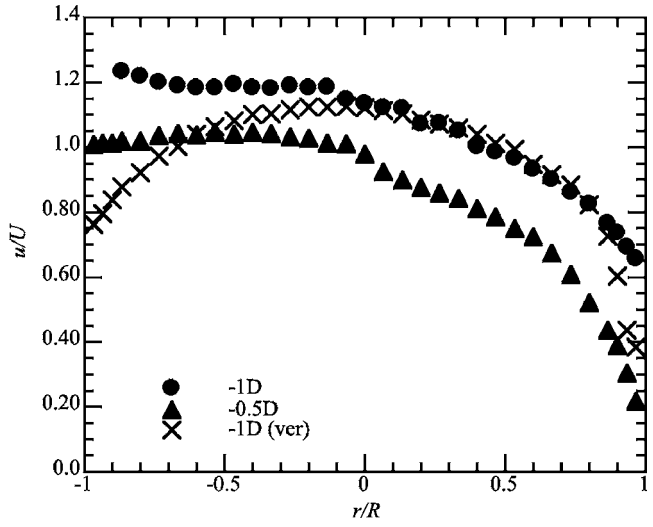

Fig. 18 Radial profiles of mean axial velocity in the bifurcation region of the round tee for Re=32,000 and Q_1/Q_3=50%: –1 D (○), –0.5 D(△); Vertical cross-stream profile at –1 D (×)

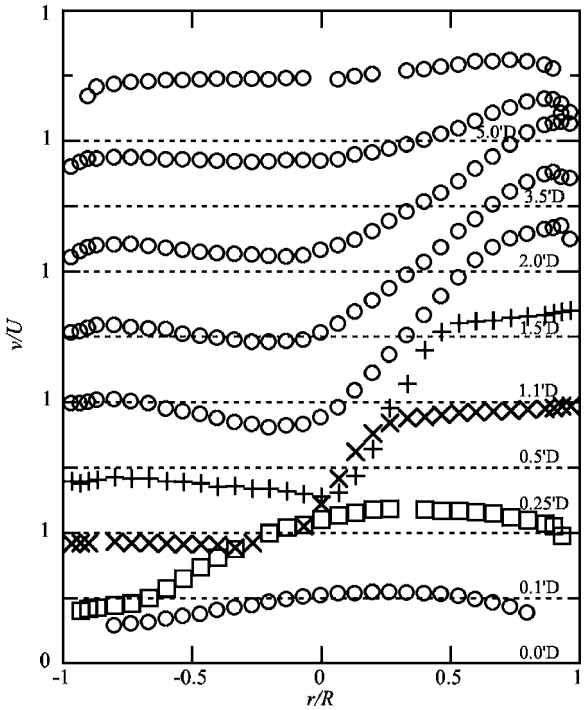

Fig. 20 Radial profiles of the longitudinal velocity in the branch pipe of the round edge tee flow for Re=32,000 and Q_1/Q_3=50%

and although the differences relative to the sharp tee data in Fig. 13 are larger than in the bifurcation region, these differences in rms velocities are too close to the measurement uncertainty and clearly insufficient to have a measurable impact on the mean flow, and by consequence on the loss coefficient K_{32} at this medium/high Reynolds number.

In the branch pipe the mean flow showed a shorter recirculation for the round edge tee and the rms velocities in Fig. 23, and their comparison with the corresponding results for the sharp tee of Fig. 14, are consistent with these findings. Looking at the turbulence profiles, and especially at the streamwise component (v'/U), the following sequence of events is observed: At the beginning of the branch pipe ($0.0'-0.5'$ D) the levels of turbulence in both the

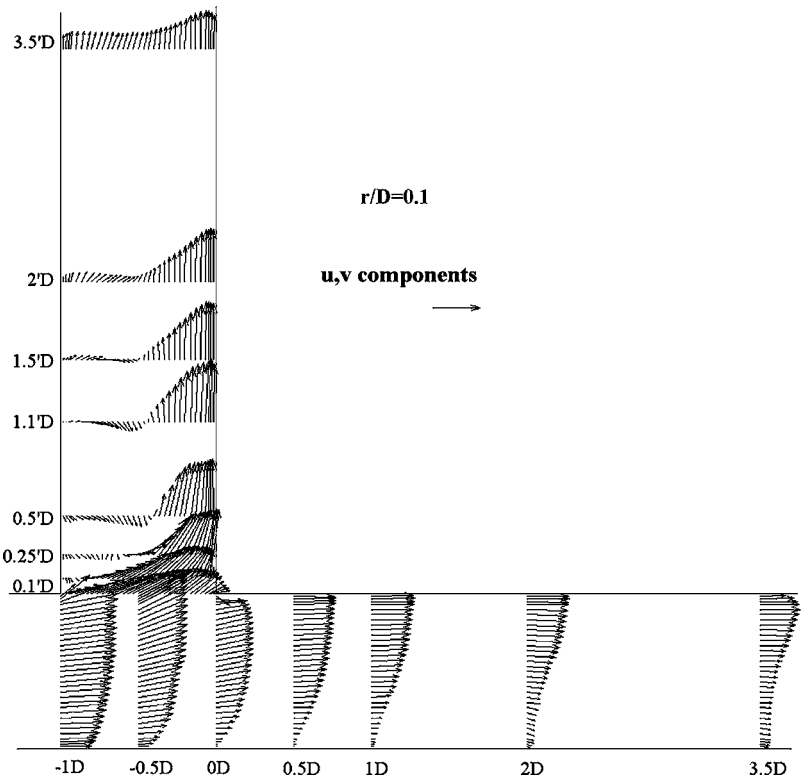

Fig. 19 Vector plot of the mean velocity in the horizontal diametric plane *x-y* of the rounded corner tee junction for Re=32,000 and Q_1/Q_3=50%. Vector scale corresponds to u/U=1.

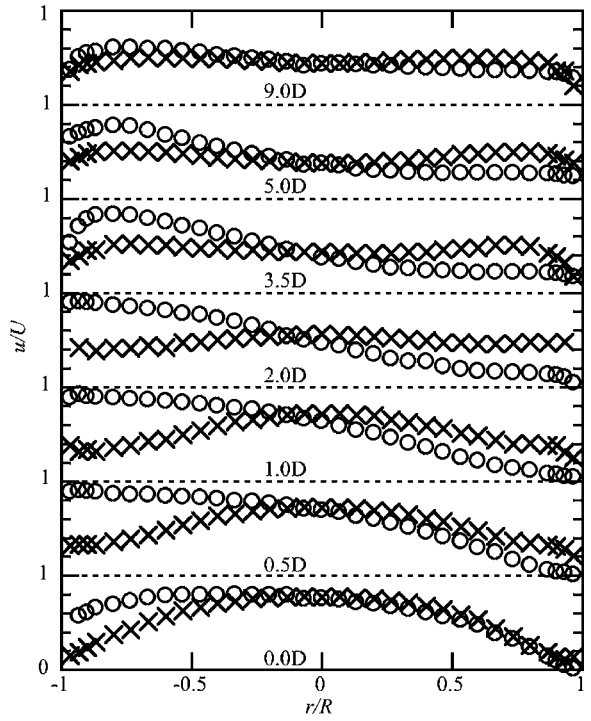

Fig. 21 Radial profiles of streamwise velocity in the outlet pipe of the round-edge tee for Re=32,000 and Q_1/Q_3=50%: ○—measurements in horizontal plane; ×—measurements in vertical plane

square and round tees are similar. At 1.1′ D the turbulence in the region $-0.5 \leqslant r/R < 1$ for the round tee is clearly higher than for the sharp tee. At this plane (1.1′ D) the peak velocities in the downstream wall jet were also seen for the round tee geometry (in Sec. 3.2.2). The higher turbulence enhances flow mixing and reduces the size of the recirculating flow, as is typical in other situations with separated flow such as in sudden expansion flows [38]. At 1.5′ D the levels of turbulence in the region $-1 < r/R \leqslant +0.5$ are similar for both geometries, but higher elsewhere for the round tee. Note that the length of the attached recirculation for the round tee is around 1.5′ D and that for the sharp tee is 2.0′ D. Henceforth, the flow along the upstream wall becomes attached for the round tee and the turbulence decreases on going downstream during flow redevelopment, whereas for the sharp tee turbulence continues to increase until 2.0′ D, when the recirculation region separates from the upstream wall. This is obvious when comparing the profiles measured at 2.0′ D, where the round tee has everywhere a lower turbulence than the sharp tee, and also further downstream at 3.5′ D.

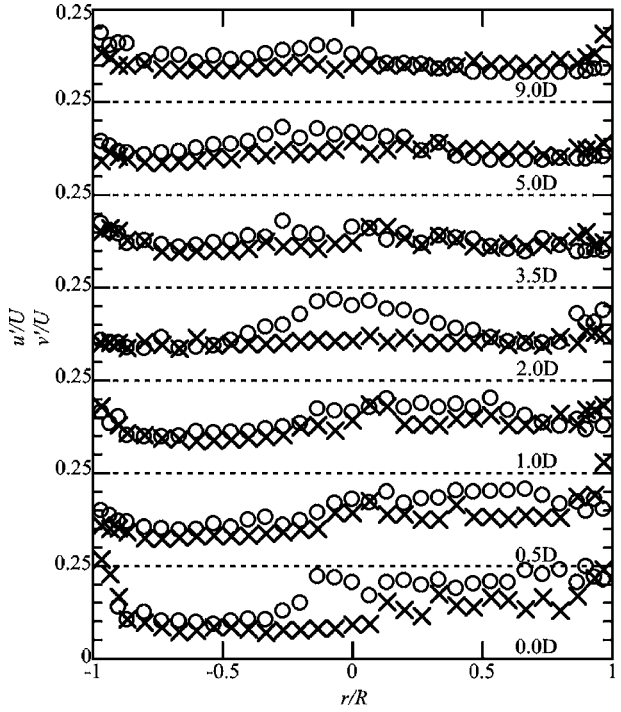

Fig. 22 Horizontal cross-stream profiles of u'/U (○) and v'/U (×) velocities in the outlet pipe of the round-edge tee for Re=32,000 and Q_1/Q_3=50%

The recirculation in the branch pipe is the main flow characteristic responsible for the dissipation of energy in the tee, hence its decrease in size and strength, due to the higher levels of turbulence in the branch pipe, has a positive effect in the reported reduction of K_{31}.

4 Conclusions

Detailed measurements of pressure variation, mean, and turbulent velocities were carried out for the flow of water in two 90 deg tee junctions with sharp and rounded edges. The detailed mean and turbulent velocity fields were measured for a flow rate ratio of 50% and inlet Reynolds numbers of 32,000 and 30,000, respectively. In both geometries, the loss coefficient of the branched flow was higher than for the straight flow, as expected, because of flow separation in the branch pipe and the absence of separation in the main outlet duct. Rounding the edge of the junction (r/R =0.1) lead to higher turbulence in the branch pipe which resulted in a shorter, thinner, and weaker recirculation bubble region, thus reducing the loss coefficient of the branched flow.

Rounding the corner also did not affect the characteristics of the flow going into the outlet straight pipe at Re≈31,000, expressing the current behavior of common turbulent flows. Moreover, the increase in dissipation in the branched flow coefficient and in terms of the total energy loss (K_D) is enough to justify that the rounded tee is obviously more efficient for all the investigated Reynolds numbers.

Acknowledgment

The authors are grateful to JNICT who funded this work through project PBIC/C/CEG/2440/95 and are also thankful to A. Schulte who carried out some of the initial measurements and helped to set-up the rig.

Nomenclature

B_T = systematic uncertainty of variable T
D_1, D_2, D_3 = diameters of pipes 1, 2, and 3
E_T = total uncertainty of variable T
f_1, f_2, f_3 = Darcy friction factor for fully developed pipe flow in pipes 1, 2, and 3
k = turbulent kinetic energy
K_{31} = loss coefficient in tee flow from the inlet to the branch pipe, Eq. (5)
K_{32} = loss coefficient in tee flow from the inlet to the straight outlet pipe, Eq. (6)
K_D = total loss coefficient of bifurcation, Eq. (9)
L_1, L_2, L_3 = lengths of pipes 1, 2, and 3
p = pressure
P_T = precision uncertainty of variable T
Q_1, Q_2, Q_3 = flowrate in pipes 1, 2, and 3
Re = Reynolds number based on inlet pipe diameter and bulk velocity

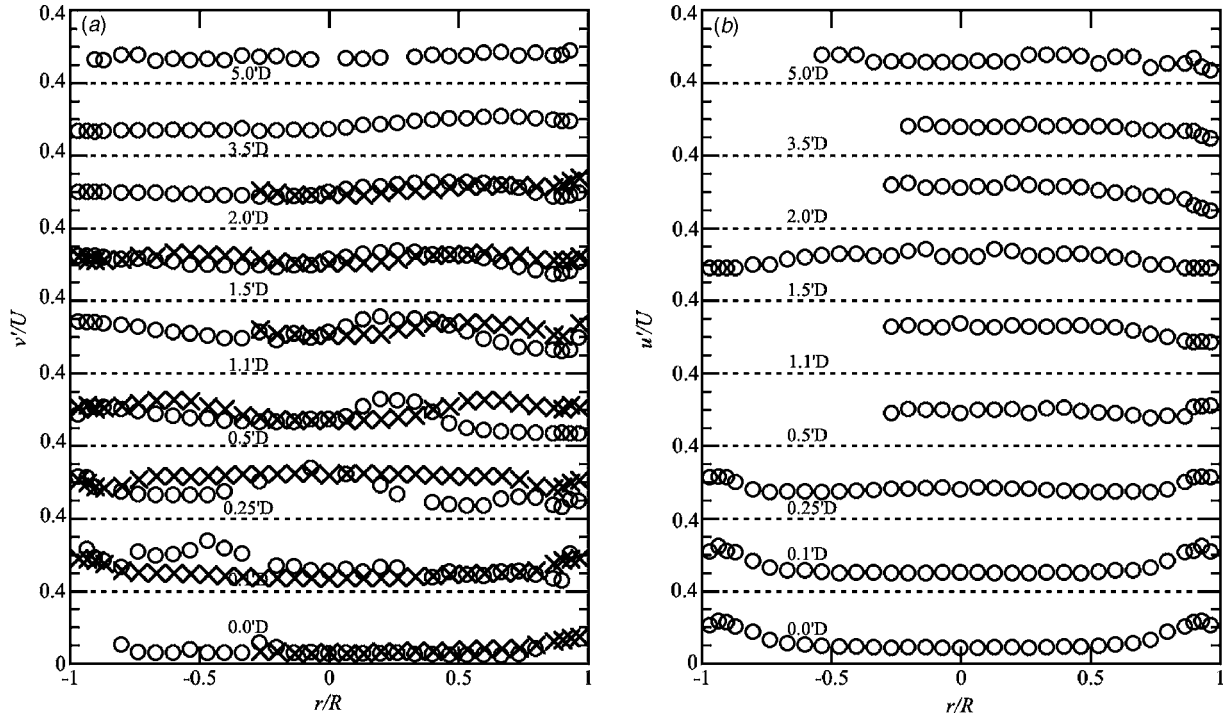

Fig. 23 Radial profiles of v'/U and u'/U in the branch pipe of the round-edge tee for Re=32,000 and Q_1/Q_3=50%. (*a*) v'/U (○—horizontal profile; ×—vertical profile); (*b*) u'/U (vertical cross-stream profile).

u = local mean (time-average) velocity in x direction (streamwise direction for inlet and straight outlet pipes and radial direction, at horizontal diametric plane, for branch pipe)

u' = local rms velocity in x direction (streamwise direction for inlet and straight outlet pipes and radial direction, at horizontal diametric plane, for branch pipe)

$\overline{u'^2}$ = normal Reynolds stress in x direction

U = bulk velocity

v = local mean (time-average) velocity in y direction (radial direction at horizontal diametric plane for the inlet and straight outlet pipes and streamwise direction for branch pipe)

v' = local rms velocity in y direction (radial direction at horizontal diametric plane for the inlet and straight outlet pipes and streamwise direction for branch pipe)

$\overline{v'^2}$ = normal Reynolds stress in y direction

w = local mean velocity in z direction

w' = local rms velocity in z direction

$\overline{w'^2}$ = normal Reynolds stress in z direction

Greek

α = energy shape factor

ϵ = rate of dissipation of k

Δp = pressure difference

ρ = fluid density

Subscripts

1 = refers to outlet branch pipe

2 = refers to outlet straight pipe

3 = refers to inlet pipe

References

[1] White, F. M., 1999, *Fluid Mechanics*, 4th ed., McGraw-Hill, New York.

[2] Vogel, G., 1926, 1928, "Investigation of the Loss in Right-Angled Pipe Branches," *Mitt. Hydraulischen Instituts der Tech. Hoschul. Munchen*, n. 1, 75-90 (1926), n. 2, 61-64 (1928) (translation by Voetsch, C. Technical Memorandum n. 299, US Bureau of Reclamation, 1932).

[3] Gardel, A., 1957, "Les Pertes de Charge Daus les Écoulements au Travers de Branchements en Té," Bull. Tech. Suisse Romande, **9**(4), pp. 123–130.

[4] Gardel, A., 1957, "Les Pertes de Charge Dansles Écoulements au Travers de Branchements en Té," Bull. Tech. Suisse Romande, **10**(5), pp. 143–148.

[5] Katz, S., 1967, "Mechanical Potencial Drops at a Fluid Branch," Trans ASME, paper 67, pp. 732–736.

[6] Iwanami, S., Suu, T., and Kato, H., 1969, "Study on Flow Characteristics in Right-Angled Pipe Fittings," Bull. Jpn. Soc. Mech. Eng., **12**(53), pp. 1041–1050.

[7] Maia, R. J., 1992, "Numerical and Experimental Investigations of the Effect of Local Losses in Piping Systems. Methods and Techniques for its Systematic Investigation. The Specific Case of the Flow in a 90 deg Tee Junction (*in Portuguese*)," PhD thesis, University of Porto, Portugal.

[8] Sierra- Espinosa, F. Z., Bates, C. J., and O'Doherty, T., 2000a, "Turbulent Flow in a 90 deg Pipe Junction. Part 1: Decay of Fluctuations Upstream the Flow Bifurcation," Comput. Fluids, **29**, pp. 197–213.

[9] Sierra- Espinosa, F. Z., Bates, C. J., and O'Doherty, T., 2000b, "Turbulent Flow in a 90 deg Pipe Junction. Part 2: Reverse Flow at the Branch Exit," Comput. Fluids, **29**, pp. 215–233.

[10] Páal, G., Maia, R., and Pinho, F. T., 2003, "Numerical Predictions of Turbulent Flow in a 90 deg Tee Junction," *Proc. 12th Int. Conf. on Modeling Fluid Flow.* Budapest, Hungary, 3–6 September, paper IFO-31, pp. 573–580.

[11] Menter, F., 1994, "Two-Equation Eddy Viscosity Turbulence Models for Engineering," AIAA J., **32**, pp. 1598–1605.

[12] Boldy, A. P., 1970, "Performance of Dividing and Combining Tees," *BHRA Technical Report 1061*.

[13] Ito, H., and Imai, K., 1973, "Energy Losses at 90 deg Pipe Junctions," *Journal of The Hydraulics Division, Proceedings of ASCE*, 99, HY9.

[14] Miller, D. S., 1986, Internal Flow Systems. *BHRA Fluid Engineering*, Cranfield, UK, 3rd ed.

[15] Katsaounis, A., Aust, E., Fürst, H. D., and Schultheiss, G. F., 1983, "Pressure Drop in Tee-Junctions with Liquids and Gas-Liquids," *Proc. 21st National Heat Transfer Conference*, Seattle, pp. 139–146.

[16] Reimann, J., and Seeger, W., 1986, "Two-Phase Flow in a Tee-Junction With a Horizontal Inlet, Part II: Pressure Differences," Int. J. Multiphase Flow, **12**, pp. 587–608.

[17] Seeger, W., Reimann, J., and Müller, U., 1985, "Phase-Separation in a T-Junction With a Horizontal Inlet," *2nd Int. Conference on multi-phase flow*, paper A2, London.

[18] Azzopardi, B. J., and Rea, S., 1999, "Modeling the Split of Horizontal Annular Flow at a T-Junction," Chem. Eng. Res. Des., **77**(A8), pp. 713–720.

[19] Azzopardi, B. J., and Rea, S., 2001, "The Split of Horizontal Stratified Flow at a Large Diameter T-Junction," Chem. Eng. Res. Des., **79**(A4), pp. 470–476.

[20] Issa, R. I., and Oliveira, P. J., 1994, "Numerical Prediction of Phase Separation in Two-Phase Flow Through T-Junctions," Comput. Fluids, **23**, pp. 347–372.

[21] Carr, R. T., and Kotha, S. L., 1995, "Separation Surfaces for Laminar Flow in Branching Tubes — Effect of Reynolds Number and Geometry," J. Biomech. Eng., **117**, pp. 442–447.
[22] Khodadadi, J. M., 1990, "Wall Pressure and Shear Stress Variations in a 90 deg Bifurcation During Pulsatile Laminar Flow," J. Fluids Eng., **113**, pp. 111–115.
[23] Moravec, S., and Liepsch, D., 1983, "Flow Investigations in a Model of a Three-Dimensional Human Artery with Newtonian and non-Newtonian Fluids— Part I," Biorheology, **20**, pp. 745–759.
[24] Rindt, C. C. M., and van Steenhoven, A. A., 1996, "Unsteady Flow in a Rigid 3D Model of the Carotid Artery Bifurcation," ASME J. Biomech. Eng., **118**, pp. 90–96.
[25] Ravensbergen, J., Krijger, J. K. B., Hillen, B., and Hoogstraten, H. W., 1995, "Merging Flows in an Arterial Confluence: The Vertebro-Basilar Junction," J. Fluid Mech., **304**, pp. 119–141.
[26] Coleman, H. W., and Steele, W. G., 1999, *Experimentation and uncertainty analysis for engineers*, 2nd ed., Wiley, New York.
[27] Costa, N. F. P., 2003, "Pressure Losses in Tee-Junctions: The 60 deg Bifurcation," (in Portuguese), MSc thesis, FEUP, University of Porto.
[28] Stieglmeier, M., and Tropea, C., 1992, "A Miniaturized, Mobile Laser-Doppler Anemometer," Appl. Opt., **31**(21), pp. 4096–4105.
[29] Albrecht, H. E., Borys, M., Damaschke, N., and Tropea, C., 2003, *Laser-Doppler and Phase-Doppler Measurement Techniques*, Springer-Verlag, Berlin.
[30] Durst, F., Melling, A., and Whitelaw, J. H., 1981, *Principles and Practice of Laser-Doppler Anemometry*, 2nd ed., Academic, London.
[31] Laufer, J., 1954, "The Structure of Turbulence in Fully Developed Pipe Flow," *National Bureau of Standards*, Report 1154.
[32] Lawn, C. J., 1971, "The Determination of the Rate of Dissipation in Turbulent Pipe Flow," J. Fluid Mech., **48**, pp. 477–505.
[33] Townes, H. W., Gow, J. L., Powe, R. E., and Weber, N., 1972, "Turbulent Flow in Smooth and Rough Pipes," J. Basic Eng., **94**, pp. 353–362.
[34] Wei, T., and Willmarth, W. W., 1989, "Reynolds Number Effects on the Structure of a Turbulent Channel Flow," J. Fluid Mech., **204**, pp. 57–95.
[35] Durst, F., Jovanovic, J., and Sender, J., 1995, "LDA Measurements in the Near Wall Region of a Turbulent Flow," J. Fluid Mech., **295**, pp. 305–335.
[36] Hinze, J. O., 1975, *Turbulence*, 2nd ed., McGraw-Hill, New York.
[37] Heitor, M. V., Taylor, A. M. K. P., and Whitelaw, J. H., 1987, "The Interaction of Turbulence and Pressure-Gradients in a Baffle-Stabilized Premixed Flame," J. Fluid Mech., **181**, pp. 387–413.
[38] Castro, O. S., and Pinho, F. T., 1995, "Turbulent Expansion Flow of Low Molecular Weight Shear—Thinning Solutions," Exp. Fluids, **20**, pp. 42–55.